IEEE Access
Multidisciplinary | Rapid Review | Open Access Journal

Received 24 June 2024, accepted 4 July 2024, date of publication 10 July 2024, date of current version 18 July 2024.

Digital Object Identifier 10.1109/ACCESS.2024.3426052

RESEARCH ARTICLE

Data-Driven Multiperiod Optimal Power Flow for Power System Scheduling Considering Renewable Energy Integration

REHMAN ZAFAR, (Member, IEEE), AND IL-YOP CHUNG, (Member, IEEE)
School of Electrical Engineering, Kookmin University, Seongbuk-gu, Seoul 02707, Republic of Korea

Corresponding author: Il-Yop Chung (chung@kookmin.ac.kr)

This work was supported in part by Korea Institute of Energy Technology Evaluation and Planning (KETEP) grant funded by Korean Government [Ministry of Trade, Industry and Energy (MOTIE)] under Grant 2019371010006B, and in part by the Information Technology Research Center (ITRC) Support Program Supervised by the Institute for Information and Communications Technology Planning and Evaluation (IITP) under Grant RS-2023-00259004.

ABSTRACT Integrating renewable energy sources (RESs) into electric power systems is environmentally beneficial; however, it also introduces operational challenges. The multiperiod optimal power flow (MP-OPF) problem becomes increasingly complex owing to the variability and uncertainty in RESs power output and load demand. To ensure system stability and reliability, other conventional generators must quickly adapt their output to counter fluctuations in RESs and mitigate network congestion. In this study, we propose a novel approach utilizing a long short-term memory recurrent neural network (LSTM-RNN) to address the MP-OPF problem. The LSTM-RNN's capability to handle time-series data enables fast and accurate predictions. By formulating the MP-OPF as a sequence-to-sequence learning problem, we train the LSTM-RNN to map input data (load demand, renewable generation) to output data (generator output, RESs injection) to meet power network constraints while simultaneously achieving economic power dispatch to generators. Additionally, we perform the post-processing on the output of LSTM-RNN results to obtain a feasible power generation schedule at each time step and to analyze network congestion and RESs curtailment. Furthermore, the proposed approach is demonstrated on the IEEE-39 bus system with time-series data, achieving highly accurate OPF solutions. Computation time is approximately 160 times faster than conventional solver.

INDEX TERMS Deep learning, generation scheduling, LSTM-RNN, optimal power flow, renewable energy integration.

ACRONYMS AND NOMENCLATURE

ACRONYMS

RESs	Renewable energy sources.
OPF	Optimal power flow.
MP-OPF	Multiperiod optimal power flow.
LSTM-RNN	Long short-term memory recurrent neural network.
DNN	Deep neural network.
SCOPF	Security-constrained optimal power flow.
GNNs	Graph neural networks.
ELM	Extreme learning machines.
CNN	Convolutional neural network.
FCNN	Fully connected neural networks.
DRL	Deep reinforcement learning.
S2S	Sequence-to-sequence.
RMSE	Root mean square error.
NRMSE	Normalize root mean square error.
MAE	Mean absolute error.
NMAE	Normalize mean absolute error.
PTDF	Power transfer distribution factors.
ESS	Energy storage system.

The associate editor coordinating the review of this manuscript and approving it for publication was Hazlie Mokhlis.

NOMENCLATURE

$P_{g,i}^{\min}$, $P_{g,i}^{\max}$	Minimum and maximum active power generation limits of *ith* generator.
$Q_{g,i}^{\min}$, $Q_{g,i}^{\max}$	Minimum and maximum reactive power generation limits *ith* generator.
$R_{g,i}^{up}$, $R_{g,i}^{down}$	Ramp-up and ramp-down limits of the *ith* generator.
$P_{d,j}^{t}$, $Q_{d,j}^{t}$	Active and reactive power absorbed at bus j at a time t.
$P_{g,j}^{t}$, $Q_{g,j}^{t}$	Active and reactive generated power at bus j at time t.
V_{j}^{t}, V_{k}^{t}	Voltages at bus j and k at time t.
$Y_{j,k}^{t}$	Admittance between bus j and k at time t.
$\theta_{j}^{\min}$, $\theta_{j}^{\max}$	Minimum and maximum voltage angle limits at bus j.
$V_{j}^{\min}$, $V_{j}^{\max}$	Minimum and maximum voltage limits at bus j.
$F_{l}^{\max}$	Maximum capacity of the line l.
θ_{j}^{t}	Voltage angle limits at bus j at time t.
F_{l}^{t}	Line flows for line l from and to the bus at a time t.
$P_{g,i}^{t}$	Active power of the i_{th} generator at a time t.
$Q_{g,i}^{t}$	Reactive power of the i_{th} generator at a time t.
α, β, γ	Cost coefficients of the *ith* generator.
P_{d}^{t}	Power demand input to LSTM-RNN network at time t.
$P_{g,RESs}^{t}$	RES generation input to LSTM-RNN network at time t.
$P_{pr,i}^{t}$	Predicted generator dispatch output of LSTM-RNN network at time t.
$P_{inj,RESs}^{t}$	Predicted RES injection power output of LSTM-RNN network at time t.
ψ_{i}^{a}, ψ_{i}^{p}	Observed and predicted data points.
$\overline{\psi^{a}}$	Average observed value.
f_{l}^{t}	Calculated flow based on the predicted dispatch in line l.
$PTDF_{ij,sr}$	PTDF factor from source bus s to receiving bus r for line l.
$P_{pr,sr}^{t}$	Power injection at source bus s, and received at receiving bus r.
x_{ij}	Reactance of the line connecting the bus i and j.
κ	Terms from inverse of the admittance matrix.
$P_{curtailed,RESs}^{t}$	Curtailed power value for RES.
$P_{g,m,RESs}^{t}$	Available power of the mth RES.
$P_{inj,m,RESs}^{t}$	Injected RES power of the mth RES.

I. INTRODUCTION

Renewable energy sources (RESs) are increasingly being integrated into electric power systems owing to their environmental and economic benefits. Despite the fact that this integration is advantageous, it requires the development of novel approaches in order to solve operational issues such as volatility and reliability of the system caused by the inherent variability and uncertainty in RESs power output and load demand. In order to develop a suitable solution, research is required in this area. Furthermore, it is challenging for power system operators to balance electricity supply and demand in real time. To maintain stability and reliability in power system operation, other conventional generators need to provide sufficient flexibility to the power system by quickly adjusting their operating points to compensate for the variability introduced by RES generators [1]. Moreover, the integration of RESs results in network congestion because of excessive surplus power generation, which can lead to various system operation problems, such as power outages, line overloading, and voltage and frequency instability [2]. To deal with such operational issues, power system operators use optimal power flow (OPF) analysis to achieve secure and economic operation conditions for the entire power systems. OPF analysis was introduced in the early 1960s to optimize the dispatch of power generation and to control the flow of electricity in the transmission network while satisfying various operational and physical constraints [3], [4]. However, the OPF problems become challenging when the power system size increases owing to the increasing complexity of the objective function with a large amount of equality and inequality constraints.

Recently, with variable generation from RES and load demand, it has become more cumbersome to solve the OPF problem. A large number of scenarios and cases must be analyzed, requiring large amounts of computation to obtain the solution. Additionally, with the involvement of the time-varying RESs and load, the solution needs to consider the temporal coupling of the variables over the time horizon, which results in a multiperiod optimal power flow (MP-OPF) formulation [5]. For instance, temporal dependence is inevitable in adding the ramping constraints of generators [6]. Therefore, MP-OPF becomes a more comprehensive solution for operation. However, this makes the OPF problem more complex, nonlinear, and nonconvex, which requires substantial time to solve. Furthermore, real-time operation requires solutions in time which is crucial to avoid system failure and cascaded blackout. Therefore, a fast and optimal system scheduling solution that can identify and manage the system on time is crucial. Given these complexities and requirements, there is a pressing need for more adaptable and quicker computational methods, motivating our exploration of data-driven machine learning algorithms to efficiently manage these challenges.

Recent studies have focused on investigating the use of data-driven machine learning algorithms to enhance the effective application of OPF. In learning-based approaches, machine learning or deep learning algorithms are used to learn the mapping between power system inputs and the corresponding optimal power flow solutions. The learning process involves training the machine or deep learning models using a set of labeled training data (supervised learning),

which consists of input-output pairs. It helps obtain the near-to-optimal solution with less computation time.

As the MP-OPF problem may considerably increase the computation time for large systems when applied for a long time horizon, the use of the conventional OPF tool may be restricted. To this end, applying machine learning algorithms in MP-OPF has the potential to predict reliable solutions in less time compared to conventional methods. Moreover, learning-based algorithms can substantially reduce the computational time required to solve the MP-OPF problem, which is essential for power systems.

Owing to the advantage of the fast and reliable solution acquisition of the learning based methods and to overcome the restrictions of conventional OPF, we propose an MP-OPF based on long short-term memory recurrent neural network (LSTM-RNN). This approach aims to provide timely solutions essential for system stability and suitable to handle the temporal dynamics inherent in MP-OPF problems. Furthermore, the proposed approach helps obtain fast power generation schedules and identify congestion using the line loadings and curtailed power of RESs to manage the uncertainty of the RESs and overall operation in time. The MP-OPF problem is a time-series problem, which is a sequence of observations over time. Hence, the LSTM-RNN architecture, which is well suited for time-series predictions, is used in this study. The LSTM-RNN involves memory which allows more learning for longer-term trends, such as in time-series data [7].

Interest in learning-based OPF has been growing, and several studies have been reported in the literature [8]. Herein, we summarize the key findings and methodologies employed in various learning-based OPF studies as we review the relevant literature. In [9], the authors employed a deep neural network (DNN) model for the OPF problem using the load demand as the model inputs and power dispatch and voltage as outputs. They achieved faster computation speed and reasonable precision compared to those using traditional OPF solvers; the solution was feasible and tested on various network cases. Similarly, [10] proposed DNN-based approach for security-constrained OPF (SCOPF) problem. By taking load data as input and predicting real-power dispatch, in comparison to conventional solvers, it delivered feasible solutions with less than 0.2% optimality loss and a much shorter computation time. Reference [11] used a DNN-based OPF approach focusing on identifying congestion and calculating RESs curtailment. The authors used load demand and RESs power generation as input, and generation scheduling, congestion identification, and RESs power injection as output. The method reported an error rate of less than 1% and considerably shorter computation time. For further details on DNN-based OPF, readers may refer to [12], [13], [14], and [15].

In [16], a physics-informed neural network is presented to estimate the OPF solution for a given demand. The framework incorporates power flow equations during the neural network training, resulting in higher prediction accuracy with fewer data points. Moreover, the paper introduces a method to minimize worst-case constraint violations in the OPF problem. Reference [17] proposed a data-driven OPF approach that uses extreme learning machines (ELM) to provide faster results while maintaining acceptable accuracy. The speed of OPF computations was significantly boosted by their method, which outperformed traditional solvers by a factor of more than 100. In [18], a novel model based on neural networks and random forests was presented for SCOPF. The approach used multitarget regression and local information to predict power generation dispatch. The dataset included load data, contingency scenarios, and transmission-line data. Various AI algorithms for mapping OPF were presented in [19], and gradient-boosting regression had the best performance in terms of accuracy and computational time. The input was load demand, and the outputs were real and reactive power dispatch and voltage levels. Some network constraints were violated, even though more than 90% of predictions were within 5% of the true solution.

References [20] and [21] investigated warm-starting OPF using graph neural networks (GNNs) for power systems in Illinois and Texas. Load data served as input, and the output was real-power scheduling. Both studies demonstrated the superior speed of GNN-based methods compared to conventional OPF solvers. In [22], a novel approach based on a random-forest model was presented, where predicted OPF solutions were used as starting points for the solver, outperforming direct current warm and flat-start methods. In [23] and [24], the topology aware GNN for learning OPF solutions by emphasizing the use of topology information in machine learning models for OPF is proposed. In [25], authors have presented a novel framework for OPF analysis based on convolutional neural networks (CNN). and self-attention mechanism. In the proposed approach, power network rearranged the data to resemble the structure of a multi-channel image to be utilized in CNN. It helped to improve the model's ability to generalize for various power system sizes. In comparison to existing OPF algorithms, the proposed method showed better efficiency and accuracy. Similarly, the authors in [26] framed the OPF problem as both a regression and a classification problem. They examined fully connected neural networks (FCNN), CNN, and GNN for OPF, demonstrating GNNs' higher performance in cases with changeable topology.

In addition to end-to end supervised learning, there are few studies that have introduced reinforcement learning (RL to frame OPF problem with temporal constraints. For instance, in [27] and [28] the deep RL (DRL)-based OPF is presented for real-time operation. In these studies, the authors have designed the OPF problem as a safe DRL by using the constrained Markov decision process to ensure the feasibility of the solutions. Nevertheless, LSTM-RNN can have an advantage over DRL techniques because of its simpler problem design. It requires mapping the input and output based

on historical data. On the other hand, RL requires a more complex setup, including reward functions, agents, and environments. In a high-dimensional stochastic setting, designing the reward function may be a complicated procedure, and performance may become unstable [24] However, the purpose of this study is to apply and enhance the use of supervised learning for problems with temporal dependencies, such as the MP-OPF problem. RL is another field to study in depth for the OPF, and it is beyond the scope of this paper.

For further exploration of learning-based OPF, [29], [30], [31], [32] provide valuable insights. Additionally, surveys related to learning-based OPF can be found in [8] and [33]. These studies collectively showcase the growing popularity and effectiveness of AI techniques in addressing OPF challenges in power systems.

Notably, the literature focuses on single period or snapshot OPF studies using machine learning and deep learning techniques. There is a need to integrate the temporal dependencies in the learning-based OPF solution in order to use it for real-world problems. In real case scenarios, the OPF problem needs to be solved by considering uncertainties frequently, and the problem becomes more complex if temporal information is added to it. To this end, learning-based OPF comes into play to reduce the computation time of the solution. A very few studies have applied learning-based methods to MP-OPF problems. Therefore, a novel LSTM-RNN-based approach for MP-OPF is proposed to address this gap. Furthermore, in order to ensure that the OPF solution obtained from the LSTM-RNN network satisfies load demand, network, and generation constraints, a systematic post-processing technique is proposed. Post-processing the LSTM-RNN network output results in updated feasible power generation schedules, line loadings, congestion information based on line loadings, and RES curtailment values. This approach can quickly solve the MP-OPF problem with negligible optimality loss. As the MP-OPF problem is temporal and uses time-series data, LSTM-RNN is chosen as the model because it achieves better accuracy in time-series prediction. The concept of the proposed MP-OPF is depicted in Fig. 1.

The contribution of the study is summarized as follows:

- The study proposes an LSTM-RNN-based model for solving the MP-OPF problem, which is a complex optimization problem that involves finding the power generation schedule for a given time horizon subject to various constraints. The study introduces a novel formulation of the MP-OPF problem as a sequence-to-sequence learning problem and uses LSTM-RNN to learn the mapping from the input data (such as load demand, renewable generation) to the output data (such as generator output, RESs generation injection). It helps solve the temporal and nonlinear aspects of the MP-OPF problem.
- The study proposes a post-processing method to ensure feasible solutions within the limits of constraints. Post-processing is applied to the solution obtained from the LSTNM-RNN network to obtain feasible power generation schedules, network line loadings, and RESs curtailment values. The proposed approach can provide fast and accurate solutions with negligible optimality loss compared to conventional solvers that are computationally expensive.
- The study demonstrates the effectiveness of the proposed method on the IEEE-39 bus power system using time-series data and evaluates the performance of the proposed method in terms of accuracy, feasibility, and computation time by comparing the proposed method with traditional OPF solvers.

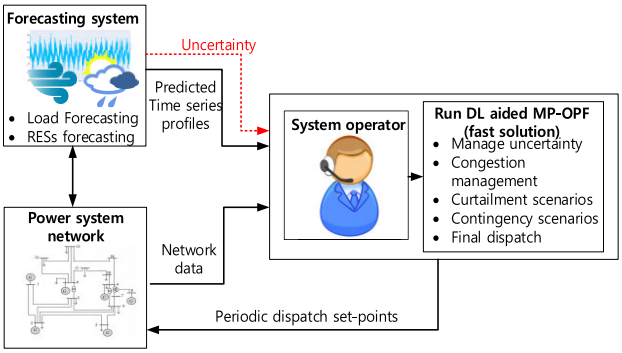

FIGURE 1. Concept of proposed AI aided MP-OPF dispatch.

The remainder of the paper is organized as follows. Section II formulates the MP-OPF problem. Section III presents the proposed approach for MP-OPF based on LSTM-RNN. Section IV describes the experiment for the case study of the IEEE-39 bus system. The Results are presented in Section V, and conclusions are drawn in Section VI.

II. FORMULATION OF MP-OPF PROBLEM

The MP-OPF problem is formulated mathematically as follows.

A. OBJECTIVE FUNCTION

The objective function $f(x)$ is defined as

$$\min_{x} f(x) = \min_{P^t_{g,i}} \left\{ \sum_{t=1}^{T} \left(\sum_{i=1}^{N_{gen}} C_g(P^t_{g,i}) \right) \right\}, \tag{1}$$

where the optimization variable x includes the output power of dispatchable generators $P^t_{g,i}$ which is defined as the generation power of the i_{th} generator at a time t; T is the overall period of the optimization; N_{gen} is the total number of the generators; and C_g is the function of the generation cost of the dispatch power.

B. POWER EQUALITY CONSTRAINTS

$$(P^t_{g,j} - P^t_{d,j}) - \mathrm{Re}\left\{ V^t_j \left(\sum_{k=1}^{N_{bus}} Y^t_{j,k} V^t_k \right)^* \right\} = 0, j = 1, \ldots, N_{bus}, \tag{2}$$

$$(Q^t_{g,j} - Q^t_{d,j}) - \mathrm{Im}\left\{ V^t_j \left(\sum_{k=1}^{N_{bus}} Y^t_{j,k} V^t_k \right)^* \right\} = 0, j = 1, \ldots, N_{bus}, \tag{3}$$

where $P^t_{g,j}$ and $Q^t_{g,j}$ are the active and reactive generated power and $P^t_{d,j}$ and $Q^t_{d,j}$ are the active and reactive power absorbed at a bus j at a time t, respectively. V^t_j and V^t_k are the voltages at bus j and k at time t, respectively; $Y^t_{j,k}$ is the admittance between bus j and k at time t. N_{bus} is the total number of buses in the system.

C. BUS VOLTAGE AND ANGLE LIMIT CONSTRAINTS

$$\theta^{\min}_j \le \theta^t_j \le \theta^{\max}_j, \quad j = 1, \ldots, N_{bus}, \tag{4}$$

$$V^{\min}_j \le V^t_j \le V^{\max}_j, \quad j = 1, \ldots, N_{bus}, \tag{5}$$

where $\theta^{\min}_j$ and $\theta^{\max}_j$ are the minimum and maximum voltage angle limits, and $V^{\min}_j$ and $V^{\max}_j$ are the minimum and maximum voltage limits at a bus j, respectively.

D. LINE CAPACITY CONSTRAINTS

Power flows in the transmission lines can be determined by the voltages and phase angles of two buses where the lines are connected. Because of the physical limits of the lines, such as the thermal limits of the lines and transformers, insulations, and protections, line flows are limited to specific capacity limits. Equation (6) expresses the constraints of line flows in MVA as follows:

$$\left| F^t_l(\theta, V) \right| \le F^{\max}_l, l = 1, \ldots, N_{line}, \tag{6}$$

where F^t_l is the line flows from and to the bus at a time t, respectively; $F^{\max}_l$ is the maximum capacity of the line; and N_{line} is the total number of lines in the power system.

E. GENERATION LIMIT CONSTRAINTS

$$P^{\min}_{g,i} \le P^t_{g,i} \le P^{\max}_{g,i}, \ i = 1, \ldots, N_{gen}, \tag{7}$$

$$Q^{\min}_{g,i} \le Q^t_{g,i} \le Q^{\max}_{g,i}, i = 1, \ldots, N_{gen}, \tag{8}$$

where $P^{\min}_{g,i}$ and $Q^{\min}_{g,i}$ are the minimum active and reactive generation limits, and $P^{\max}_{g,i}$ and $Q^{\max}_{g,i}$ are the maximum active and reactive generation limits of the *ith* generator, respectively.

F. RAMPING LIMIT CONSTRAINTS

$$P^t_{g,i} - P^{(t-1)}_{g,i} \le R^{up}_{g,i}, i = 1, \ldots, N_{gen} \tag{9}$$

$$P^{(t-1)}_{g,i} - P^t_{g,i} \le R^{down}_{g,i}, i = 1, \ldots, N_{gen} \tag{10}$$

where $R^{up}_{g,i}$ and $R^{down}_{g,i}$ are the ramp-up and ramp-down limits of the *ith* generator, respectively.

G. FUEL COST CURVE

Generator cost curves are usually presented as cubic, quadratic, or piecewise linear functions. Here, we use a quadratic fuel cost function defined as:

$$C_g(P^t_{g,i}) = \alpha + \beta . P^t_{g,i} + \gamma . (P^t_{g,i})^2, \tag{11}$$

where α, β, and γ are the cost coefficients of the *ith* generator

III. LSTM-RNN BASED MP-OPF

A. STRUCTURE OF LSTM-RNN BASED MP-OPF

In this study, we propose an MP-OPF based on LSTM-RNN for time-series operation in order to obtain generation schedule along with line loadings, RESs curtailment and congestion information. The architecture for the proposed MP-OPF based on LSTM-RNN consisting of the following four steps is shown in Fig. 2. Details of each step are explained in the subsections.

Step 1: In the first step, the dataset is created. In real systems, the historical data is obtained from the energy-management system at the system-operator end. The data should comprise historical MP-OPF dispatch solutions, load, and RESs generation. Herein, we create a dataset that includes the MP-OPF solution computed using a conventional MP-OPF solver, historical time-series load, and RESs power generation data.

Step 2: The LSTM-RNN model is then trained using the input as the time-series RESs power generation and load data while the output is the time-series generation dispatch.

Step 3: This is the inference phase, where unseen inputs are provided to the trained LSTM-RNN model to obtain the outputs. The test set is used at this stage to obtain the MP-OPF results from the trained model. A 24-h operation horizon is considered. In real-case scenarios, the input is the real load demand and renewable energy generations. Then, the trained RNN-LSTM model enables the prediction of the MP-OPF outputs.

Step 4: The obtained MP-OPF output is then moved to the post-processing phase where the transmission and equipment constraints are checked and the final output is obtained in terms of updated generation schedule, congestion scenarios, line loadings, and power curtailment values of the RESs power.

B. DATASET CREATION AND DATA PRE-PROCESSING

Dataset creation and data pre-processing is the first step of the proposed scheme. In this step, a dataset is created using time-series data which includes the load and renewable energy resource data as input data. This input data is fed into a conventional MP-OPF solver [34] and the MP-OPF solution is obtained.

The solution of the MP-OPF solver is stored as the output data. We used five years of hourly data for load and RESs data. We used the wind speed data from the NASA database for New England, USA. The load data was acquired as historical real data of the same location and scaled to the peak

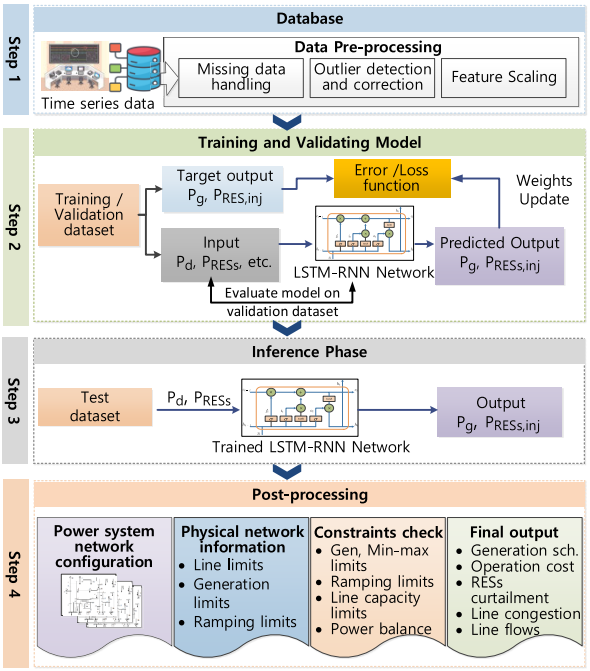

FIGURE 2. Proposed LSTM-RNN MP-OPF framework.

value of the case-study system; more detail for the dataset and time-series data analysis is provided in the case-study section. Furthermore, in this step, pre-processing was performed to handle the data outliers, feature scaling, and data division for training, validation, and testing of the proposed approach. The method to create the database is depicted in Fig. 3.

C. TRAINING OF THE LSTM-RNN MODEL

The LSTM-RNN model was trained using the training dataset. In this case, sequence-to-sequence (S2S) architecture was used for LSTM-RNN training. The architecture of the LSTM-RNN for the MP-OPF problem is shown in Fig. 4. In this approach, the sequence of the input was fed into the LSTM-RNN cells to obtain the sequence of output while minimizing the training loss. LSTM-RNN was used for the proposed model because several studies showed that it is best suitable for time-series problems. For training, hyperparameters were optimized using the validation set.

The network has various layers, such as the input layer, the output layer, the fully connected layer, and several hidden layers based on LSTM cells. The addition of more than one LSTM-based layer deepens the network and aids it in learning the temporal connections associated with the relevant time steps. The predicted result is outputted by the fully connected layer and the output layer. Inputs are fed to the LSTM layer in the form of the sequence $t \in T$ which is the time horizon as the MP-OPF period, while the feature inputs are the load and RESs presented as F. Furthermore, the total number of training examples is presented as N. After passing the examples from the network, final outputs are generated as $G_1, \ldots . G_T$.

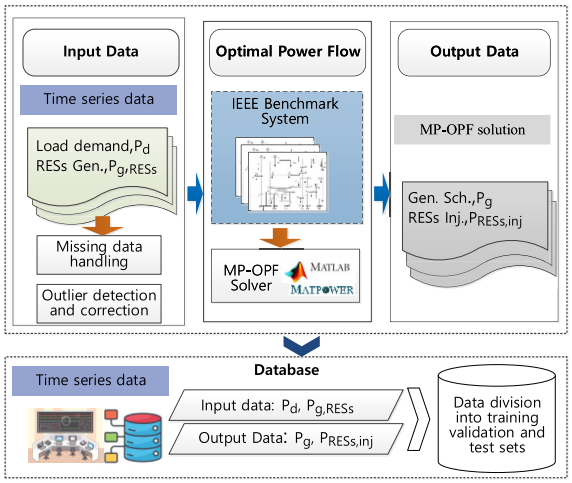

FIGURE 3. Architecture of database creation for LSTM-RNN based MP-OPF approach.

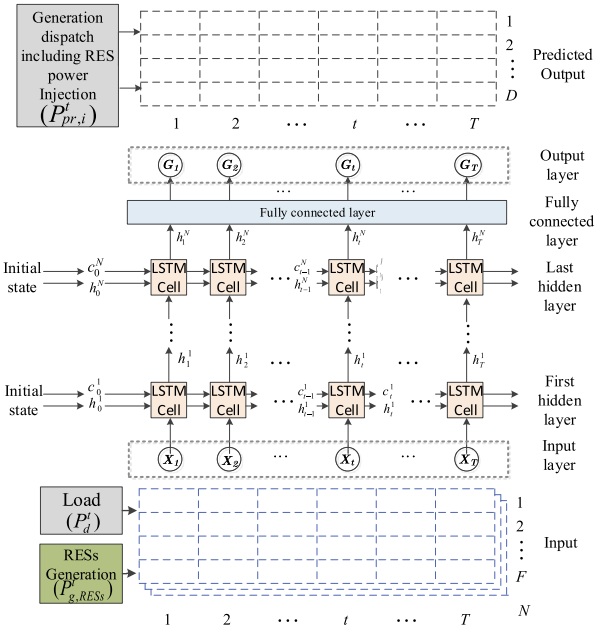

FIGURE 4. LSTM-RNN architecture for MP-OPF.

For MP-OPF, we used multiple inputs such as time-series demand P_d^t and RES generation $P_{g,RESs}^t$ for T time steps. The output consisted of the predicted generator dispatch values $P_{pr,i}^t$ including RES generation injection $P_{inj,RESs}^t$ i.e. multiple outputs for T time steps.

D. PERFORMANCE EVALUATION

To test the trained model, we used the test dataset for one year and obtained the generation schedule and including RESs power injection into the system.We compared the accuracies of test results with the validation results accuracies to prevent underfitting and overfitting of the model. Then, we fed the output into the post-processing phase for the final output. We used the following performance parameters

in this study: root mean square error (RMSE) (12), normalized RMSE (NRMSE) (13), mean absolute error (MAE) (14), and normalized MAE (NMAE) (15). The aim to utilize multiple evaluation metrics was to provide a comprehensive analysis of the model performance from different statistical perspectives, each relevant to the specific characteristics and requirementsThe RMSE and MAE are widely used metrics for regression problems; therefore, we have used these metrics for the proposed study. Normalization of these metrics is performed to evaluate the various parameters on the same scale.

$$RMSE = \sqrt{\frac{1}{N}\sum_{i=1}^{N}\left(\psi_i^a - \psi_i^p\right)^2}, \tag{12}$$

$$NRMSE = \frac{RMSE}{\overline{\psi^a}} * 100\%, \tag{13}$$

$$MAE = \frac{1}{N}\sum_{i=1}^{N}\left|\psi_i^a - \psi_i^p\right|, \tag{14}$$

$$NMAE = \frac{MAE}{\overline{\psi^a}} * 100\%, \tag{15}$$

In the above equations, ψ_i^a and ψ_i^p, are the observed and predicted data points, respectively; $\overline{\psi^a}$ is the average observed value; N is the total number of samples.

E. POST-PROCESSING PROCEDURE

The output of the LSTM-RNN model was postprocessed. The results were checked to make them feasible within the limits of constraints such as power balance, ramping limits, generation minimum and maximum power.

This was done using the information of the physical system configuration. Fig. 5. shows the flow chart of the post-processing process. The post-processing is described in the following steps.

Step 1: For generation constraints, the obtained power generation dispatch is adjusted as follows: If the obtained generation point of any generator is more than the maximum or less than the minimum power, it is adjusted to the minimum and maximum generation limits, respectively.

Step 2: If the output generating schedule does not meet the demand, the power balance is maintained by adjusting the operating points of the generators within the generation, ramping, and line-loading limits.

For example, if the total generation is less than the total load demand, then the power points of RES generators are increased, given that RES power is available and line loadings are within limits. If it is true then power is assigned to other generators (considering line, ramp-up, and generation limits) based on cost prioritization until generation balance is achieved.

Similarly, if the total generation exceeds the load demand, power is reduced, starting from the costliest generator to the cheapest until the power balance is maintained.

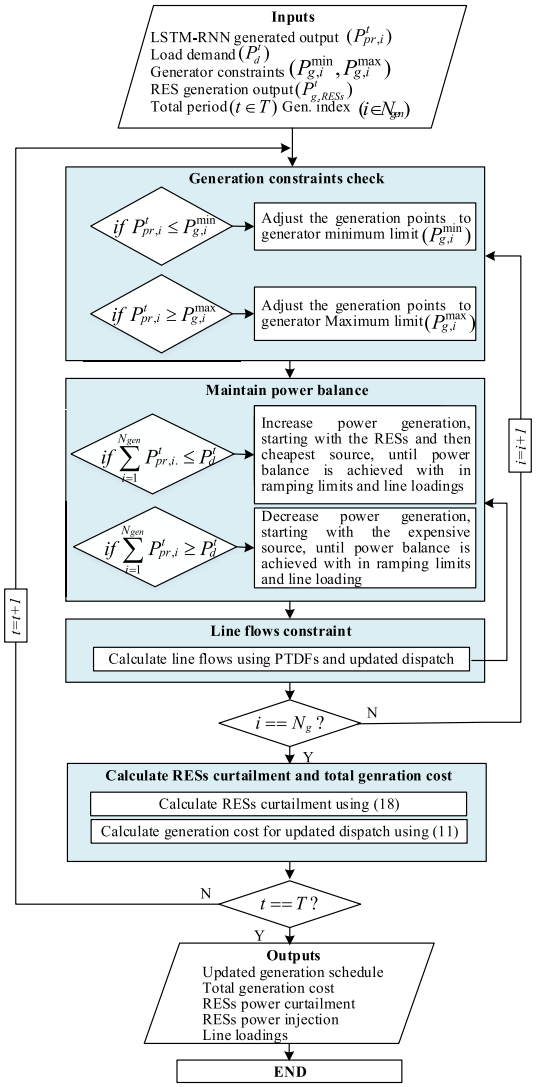

FIGURE 5. Flow-chart for the post-processing process.

The line flows are calculated based on the updated power dispatch and power transfer distribution factors (PTDF) as follows.

$$f_l^t = PTDF^*_{ij,sr} P^t_{pr,sr} \tag{16}$$

where f_l^t is the calculated flow based on the predicted dispatch in line l from bus i to j, $PTDF_{ij,sr}$ is the factor that gives the fraction of power to the network at source bus s to receiving bus r which flows over line l, $P^t_{pr,sr}$ is the power injection at source bus s, and received at receiving bus r.

In addition, PTDF is obtained from the inverse of the admittance matrix as in [27]:

$$PTDF_{ij,sr} = \frac{1}{x_{ij}}[(\kappa_{is} - \kappa_{ir}) - (\kappa_{js} - \kappa_{jr})], \tag{17}$$

where x_{ij} is the reactance of the line connecting the bus i and j, and κ terms are obtained from the inverse of the admittance matrix.

Line loadings are obtained in MW and then converted to percentage values. Line loadings also help identify congestion in the line, and early warning on overloaded lines can be obtained.

Step 3: During post-processing, the amount of RES power curtailment is the power generation from RESs minus the predicted RESs power injection by the N_r source at each time step, calculated as:

$$P^t_{curtailed,RESs} = \sum_{m=1}^{N_r} P^t_{g,m,RESs} - \sum_{m=1}^{N_r} P^t_{inj,m,RESs}, \quad (18)$$

where $P^t_{curtailed,RESs}$ is the curtailed power value, $P^t_{g,m,RESs}$ is the available power, and $P^t_{inj,m,RESs}$ is the injected power of the mth RES, respectively.

Step 4: The overall generation cost is recalculated based on the updated power generation dispatch using (11).

In summary, the updated generator schedule, total generation cost, amount of RES power curtailment, RES power injection, and line loadings are obtained as the final output after the post-processing procedure.

IV. EXPERIMENTAL SETUP

A. CASE STUDY

The case study for the proposed approach explored the IEEE 39-bus system, which is a 10-machine New England power grid [35]. The system has a transmission voltage of 345 kV and 10 generators that can produce up to 7,367 MW. The system has 21 loads with a peak demand of 6,254 MW. The network comprises 46 branches that connect the buses, including six tie lines that link three areas. A RES generator in the form of a wind farm was added on bus 18, as shown in Fig. 6.

The network data for the study was taken from [36]. The wind power and load profile in terms of time-series data are described in the following subsections.

1) LOAD DATA

The load data was acquired as historical real data of New England [37]. The data was scaled to the 6254 MW peak to match with the IEEE 39-bus system. The monthly average load pattern for the year 2020 is shown in Fig.7; the same patterns were observed for other years. Usually, peaks happen at night between 6 and 9 o'clock. The months of July and August have the most consumption.

2) WIND SPEED DATA

We used wind turbines as RESs at Bus 18 and the data for wind speed were obtained from NASA [38]. The wind speed curve with rated power, and cut-in and out speed is shown in Fig. 8. The wind speed distribution is shown in Fig. 8.

We considered a 700-MW wind farm which was assumed based on the average total rated generation of other generators which is around 700 MW. The farm comprised of 140 wind turbines generating 5 MW. The power output is calculated using the wind speed, swept area of the turbine which we considered as 12,868 m^2, and air density, which is taken as 1.225 kg/m^3

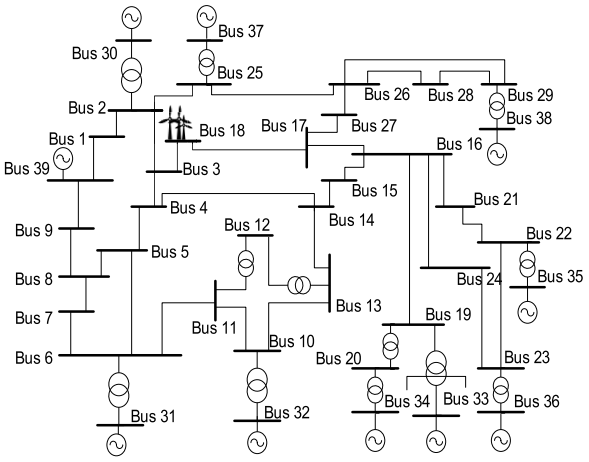

FIGURE 6. IEEE-39 bus system with RES location at Bus 18.

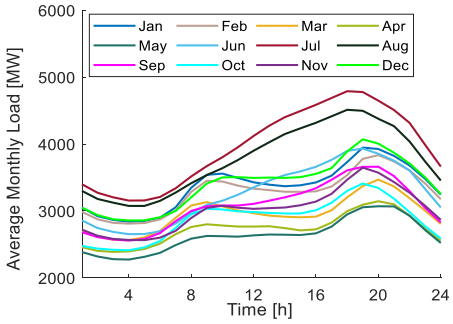

FIGURE 7. Monthly load pattern.

B. DATASET DIVISION

For MP-OPF, we used the time-series data of wind speed, and for the load data, we used five years of wind speed and power consumption data. Wind speed data were acquired from NASA. The load data were acquired from the New England region. The data were further divided into training, validation, and test sets as described in Table 1.

C. HYPERPARAMETER TUNING

To achieve the best forecasting model performance, it is crucial to fine-tune the hyperparameters that affect the computation and memory factors. In this study, we tuned the hyperparameters of the LSTM-RNN model such as the number of hidden layers, number of hidden units, dropout rate, number of epochs, optimization solver, learning rate, and scaling of features. Table 2 shows the optimal values of the hyperparameters for the LSTM model from the search space. The hyperparameter optimization was done by trial-and-error method.

Among the tested optimization solvers, which included ADAM, SGDM, and RMSprop, the ADAM optimizer was the most effective. The optimal values for the number of

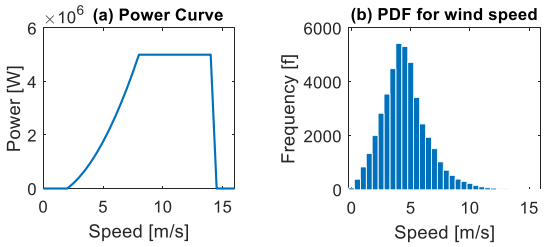

FIGURE 8. Power curve of wind turbines and wind speed distribution.

TABLE 1. Data division.

Datasets	Periods	Number of days
Training set	1 Jan 2016–31 Dec 2018	1096
Validation set	1 Jan 2019–31 Dec 2019	365
Test set	1 Jan 2020–31 Dec 2020	366

TABLE 2. Hyperparameter for LSTM-RNN based MP-OPF.

Hyperparameter	Value	Search space
Learning rate	0.001	0.0005,0.1, 0.01 and 0.001–0.005
Optimization solver	ADAM	ADAM, SGDM, RMSprop
Feature scaling	Standard	Min–Max and Standard scaler
Number of layers	2	1–15
Hidden units/layer	24	12, 24, 48, 96, 192
Number of epochs	4000	500–5000
Dropout rate	0.5	0.05–0.8

hidden layers and hidden units were 2 and 24, respectively. The standard scaler method was used for feature scaling as it yielded the best results. The dropout rate was fixed at 0.5, which also helped to prevent overfitting. Lastly, the number of epochs was set to 4000.

V. RESULTS

In this section, the results of the proposed approach are shown and discussed. Herein, the IEEE-39 bus system is used, as described in the case study. First, the results for the LSTM-RNN model are discussed, and then, the post-processing results are reported. Thereafter, a comparison between the output of the proposed approach and that of the conventional approach is performed. Finally, the computation burden is compared.

A. LSTM-RNN BASED MP-OPF TRAINING PERFORMANCE

The LSTM-RNN model is trained on the MP-OPF input and targeted outputs. The period is selected as 24 h; it produces the prediction of 24 time slots. We obtained the results for the generation scheduling and postprocessed them to obtain the line loading, RES curtailment and total generation cost. Fig. 9 shows the scatter curve fitting plot for the test set for the MP-OPF solutions, which are generation dispatch

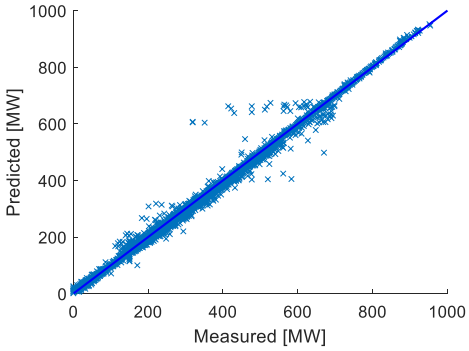

FIGURE 9. Scatter plot for the generation obtained from LSTM-RNN based MP-OPF and calculated from conventional OPF.

points (including RES generation) obtained from the conventional MP-OPF solver. These are considered measured points versus generation dispatch points obtained from the trained LSTM-RNN model.

Table 3 shows the accuracy results in terms of RMSE, NRMSE, MAE, and NMAE. The NRMSEs are <0.1% for both validation and test sets (Table 3). Results of NRMSE comparisons of the validation and test sets are shown in Fig. 10. The comparison shows that the trained network is neither underfitted nor overfitted because the accuracy is almost the same for the validation and test sets; hence, the model is well generalized.

B. LSTM-RNN-BASED MP-OPF AFTER POST-PROCESSING ACCURACY ANALYSIS

The obtained generation dispatch solutions from the trained LSTM-RNN model are post-processed and used to calculate the line loadings, RES curtailment values, and generation cost to the expected dispatch solution. Accuracies in terms of NRMSE are calculated for these parameters using the conventional MP-OPF solver values.

The accuracies of the proposed approach are shown in Table 4. The expected generation dispatch, expected generation cost, line loadings, and RES curtailment values achieved NRMSE values of 0.076%, 0.0053%, 0.196%, and 0.036%, respectively. These errors are <1% and these solutions are obtained in less than a minute for the whole year's data.Post-processing on the obtained solution is necessary to ensure that system constraints are not violated and to obtain system balance by adjusting the outputs of the generation.

C. ANALYSIS AND COMPARISON OF THE PROPOSED MP-OPF METHOD

We compared the results of the proposed study. For annual operation, Table 5 shows the comparison of total generation, cost, and RESs curtailment for the conventional OPF solver before post-processing and after post-processing.

Figs. 11(a) and 11(b) show the daily total generation comparison before post-processing and after post-processing with the conventional solver, respectively. The total generation for the conventional and LSTM-RNN trained model after

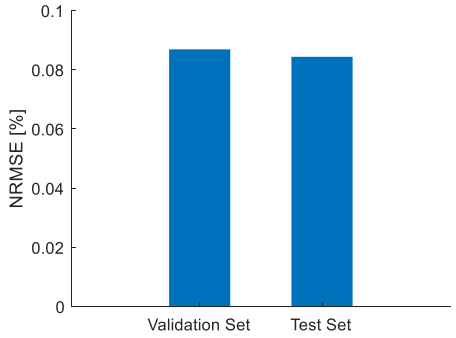

FIGURE 10. Error comparison for validation and test set.

TABLE 3. Performance evaluation for LSTM-RNN-based MP-OPF.

Performance Matrices	Validation Set	Test Set
RMSE [MW]	25.89	24.50
NRMSE [%]	0.086	0.084
MAE [MW]	35.89	37.60
NMAE[%]	0.12	0.13

TABLE 4. Performance evaluation for LSTM-RNN-based MP-OPF after post-processing.

Parameters	RMSE	NRMSE (%)
Generator power scheduling	22.21 MW	0.076
Generation cost	$ 404.40	0.0053
Line loading	27.96 MW	0.196
Curtailment	14.88 MW	0.036

TABLE 5. Comparison of the proposed and conventional methods for annual operation.

Parameters	Convention solver	Before post-processing	After post-processing
Total generation [GWh]	28063.41	27926.92	28063.41
generation cost [million$]	673.60	670.27	673.79
RESs curtailment [GWh]	15.67	46.48	21.13

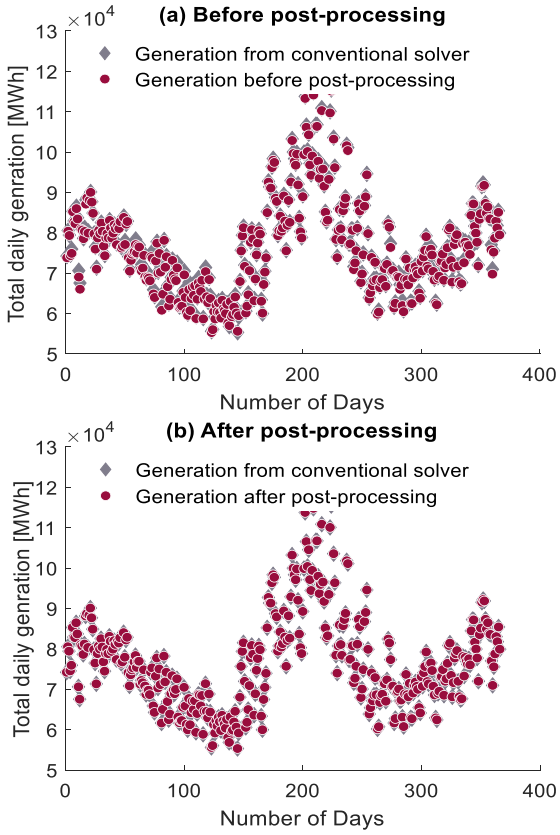

FIGURE 11. Comparison of the output generation.

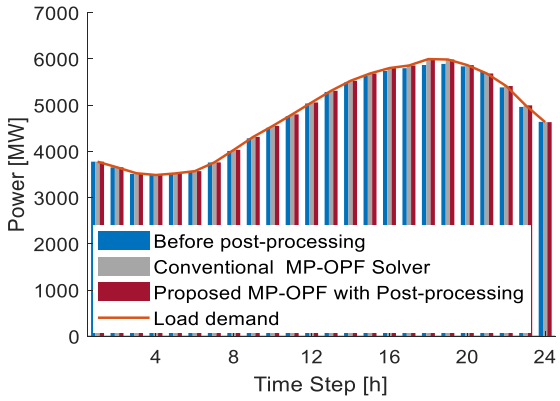

FIGURE 12. Scheduling results for conventional and proposed method for a day (209th day of test set).

post-processing has the same generation. There is no difference in generation between the conventional solver and the proposed method with post-processing. Similarly, the cost difference is also small with the percentage difference of 0.028%. However, the curtailment difference is 5.46 GWh.

Additionally, we compared the graphical results to have better insight into the proposed method. Fig. 12. shows the overall dispatch solutions obtained from the conventional MP-OPF solver and the proposed method for a day when the maximum load has been recorded (209th day of the test set).

Herein, the results are for the LSTM-RNN model output of the proposed method before post-processing. Before post-processing, in 18, 19, and 20 h, there are some shortages in the prediction of generation points. These shortages are adjusted by applying the proposed post-processing algorithm. We observed that the demand is met with the proposed method with post-processing without any shortages. In this case, the generation cost for the conventional method and the proposed method have a difference of around 0.041%.

From the same day, we also compared the dispatch of the single period to evaluate the operation of the proposed and conventional approaches. Fig. 13(a) shows the single-period dispatch results for 11 generators including one RES for hour number 18. Generator number 10 compensated for the generation by increasing its output under the limits of generation, ramp rate, and other constraints.

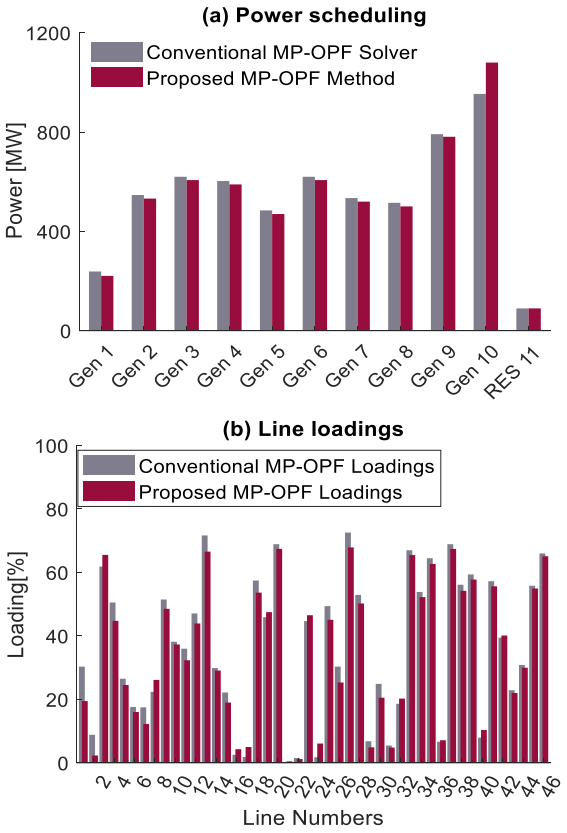

FIGURE 13. Generation scheduling and line-loading results for conventional and proposed methods for an hour (209th day, 18th hour of test set) for high-demand loading condition.

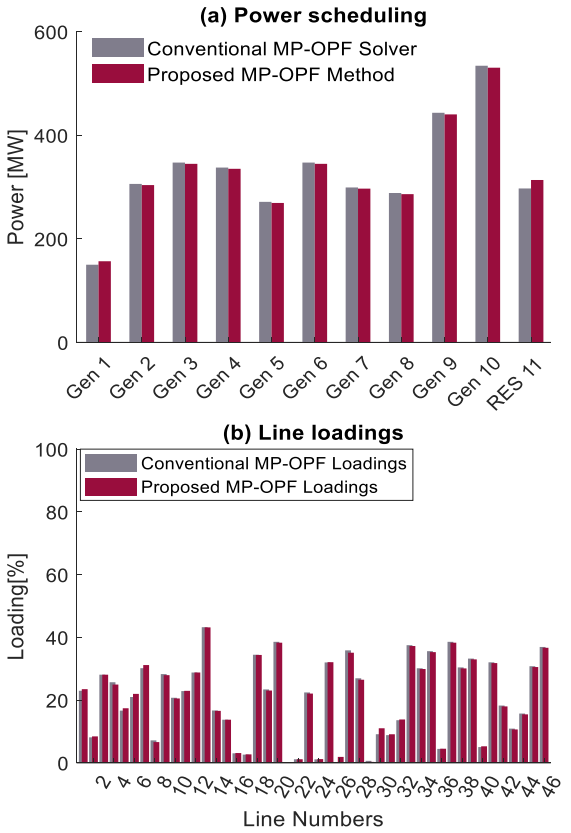

FIGURE 14. Scheduling and line loading results for conventional and proposed methods for an hour (10th day, 12th hour of test set) for large RES generation.

Overall, the obtained generation points from proposed method for generators were not considerably varied from those obtained by the conventional method. Fig. 13(b) shows the line loading of the same hour to evaluate the effects of the proposed method on line loadings. It compares the line loading of 46 lines under the conventional and proposed methods. The line-loading results show no limit violations for both methods. There are no extreme increases or decreases in line loading for the proposed solution; therefore, this is another indicator that the proposed MP-OPF method can be adopted with the advantage of fast solution acquisition for larger systems.

Similarly, the results are discussed for the scenario when there is surplus RESs power in a particular hour. In the case of total curtailment, the proposed approach showed more curtailment; however, there are some periods when there was less curtailment compared to that of the conventional solver. Therefore, to analyze such a case, the 12th hour of the 10^{th} day of the test day is discussed in terms of generation dispatch, line loadings, and RES power curtailment. Fig. 14(a) shows the generation dispatch for the conventional and proposed methods.

The line loadings are depicted in Fig. 14(b). The results of the proposed method for dispatch are quite close to those of the conventional method. In this scenario, the generation from Generator 1 and RES were slightly more than those of the conventional method.

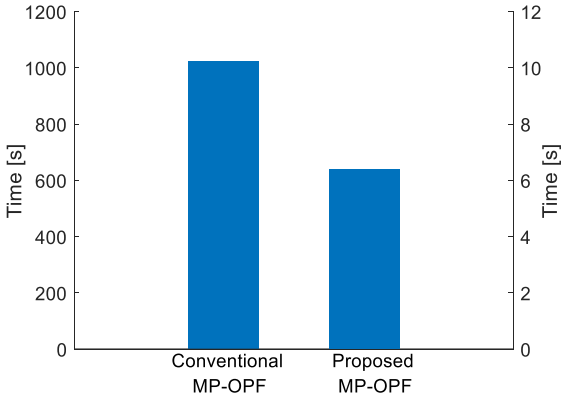

FIGURE 15. Computational time for solutions of the proposed and conventional methods.

D. COMPUTATIONAL TIME EVALUATION

For this study, simulations are performed using MATLAB 2022a on a desktop computer with i7 processor and 16 GB RAM. For the conventional MP-OPF solutions, we used MATPOWER 7.1. The computational time for the proposed and conventional methods was compared for a one-year operation. The conventional MP-OPF solver took 1023.6 seconds to obtain the solutions for a year of operation, whereas the proposed approach took just 6.39 seconds for the same, as shown in Fig. 15.

Therefore, the proposed solution method is approximately 160 times faster than the conventional solver. Moreover, the proposed approach has the advantage of fast processing with minor error of $<1\%$. Additionally, post-processing helps obtain a feasible solution without violating the thermal and generation limits and without considerable loss in overall operating cost.

VI. CONCLUSION

This study proposed an LSTM-RNN based MP-OPF approach design to obtain solutions in terms of generation dispatch, total generation cost, curtailment values, and line loadings. The model demonstrated high accuracy across all parameters, with errors below 1%. The post-processing mechanism in the proposed approach helps obtain feasible solutions by keeping the solutions within the limits of constraints. For annual operations, the proposed method demonstrated a marginal percentage difference of 0.028% in optimal cost of generation compared to conventional method. The total generation from the proposed method matched that of the conventional approach, meeting a demand of 28,063.41 GWh.

Moreover, the computational time required for a one-year operation for the proposed approach and a conventional solver was compared. The proposed approach took merely 6.39 seconds to solve the problem compared with the 1023.6 seconds taken by the conventional solver. The proposed method was approximately 160 times faster.The fast speed of the proposed method makes it a promising solution for real-time operations. It can play a vital role in addressing uncertainties related to RES and efficiently managing their impact on power systems. Moreover, the approach can be scaled to lower time resolutions, making it well suited for handling the uncertainties associated with RES in such settings.

Overall, as presented in this paper, the MP-OPF approach based on LSTM-RNN depicts both accuracy and computational efficiency, thereby making it a valuable tool for power system optimization and real-time operations with renewable energy integration.

Furthermore, future work could enhance the proposed approach by applying it to the unit commitment problem, where it could handle additional constraints other than ramping constraints, such as minimum up and down times and binary variables for unit on/off operations. This enhancement would require extensive training and a development of hybrid deep learning techniques, alongside more sophisticated post-processing algorithms. Similarly, integrating energy storage systems (ESS) would be a valuable extension of the proposed work, as it involves managing the temporal dynamics of charging and discharging states.

REFERENCES

[1] R. Rajan, F. M. Fernandez, and Y. Yang, "Primary frequency control techniques for large-scale PV-integrated power systems: A review," *Renew. Sustain. Energy Rev.*, vol. 144, Jul. 2021, Art. no. 110998, doi: 10.1016/j.rser.2021.110998.

[2] F. Monforti-Ferrario and M. P. Blanco, "The impact of power network congestion, its consequences and mitigation measures on air pollutants and greenhouse gases emissions. A case from Germany," *Renew. Sustain. Energy Rev.*, vol. 150, Oct. 2021, Art. no. 111501, doi: 10.1016/j.rser.2021.111501.

[3] J. Carpentier, "Contribution to the economic dispatch problem," *Bull. de la Societe Francoise des Electriciens*, vol. 3, no. 8, pp. 431–447, 1962.

[4] M. B. Cain, R. P. O'neill, and A. Castillo, "History of optimal power flow and formulations," *Federal Energy Regulatory Commission*, vol. 1, pp. 1–36, Dec. 2012.

[5] J. F. Marley and I. A. Hiskens, "Multi-period AC-QP optimal power flow including storage," in *Proc. Power Syst. Comput. Conf. (PSCC)*, Genoa, Italy, Jun. 2016, pp. 1–7, doi: 10.1109/PSCC.2016.7540844.

[6] Q. Gemine, D. Ernst, Q. Louveaux, and B. Cornélusse, "Relaxations for multi-period optimal power flow problems with discrete decision variables," in *Proc. Power Syst. Comput. Conf.*, Wroclaw, Poland, Aug. 2014, pp. 1–7, doi: 10.1109/PSCC.2014.7038396.

[7] J. Korstanje, *Advanced Forecasting With Python*. New York, NY, USA: Springer, 2021.

[8] F. Hasan, A. Kargarian, and A. Mohammadi, "A survey on applications of machine learning for optimal power flow," in *Proc. IEEE Texas Power Energy Conf. (TPEC)*, College Station, TX, USA, Feb. 2020, pp. 1–6, doi: 10.1109/TPEC48276.2020.9042547.

[9] X. Pan, M. Chen, T. Zhao, and S. H. Low, "DeepOPF: A feasibility-optimized deep neural network approach for AC optimal power flow problems," *IEEE Syst. J.*, vol. 17, no. 1, pp. 673–683, Mar. 2023, doi: 10.1109/JSYST.2022.3201041.

[10] X. Pan, T. Zhao, M. Chen, and S. Zhang, "DeepOPF: A deep neural network approach for security-constrained DC optimal power flow," *IEEE Trans. Power Syst.*, vol. 36, no. 3, pp. 1725–1735, May 2021, doi: 10.1109/TPWRS.2020.3026379.

[11] R. Zafar, B. H. Vu, and I.-Y. Chung, "A deep neural network-based optimal power flow approach for identifying network congestion and renewable energy generation curtailment," *IEEE Access*, vol. 10, pp. 95647–95657, 2022, doi: 10.1109/ACCESS.2022.3204803.

[12] X. Pan, "DeepOPF: Deep neural networks for optimal power flow," in *Proc. 8th ACM Int. Conf. Syst. Energy-Efficient Buildings, Cities, Transp.*, Nov. 2021, pp. 250–251, doi: 10.1145/3486611.3492390.

[13] T. Zhao, X. Pan, M. Chen, A. Venzke, and S. H. Low, "DeepOPF+: A deep neural network approach DC optimal power flow for ensuring feasibility," in *Proc. IEEE Int. Conf. Commun., Control, Comput. Technol. Smart Grids*, Tempe, AZ, USA, Nov. 2020, pp. 1–6, doi: 10.1109/SmartGridComm47815.2020.9303017.

[14] M. Kim and H. Kim, "Projection-aware deep neural network for DC optimal power flow without constraint violations," in *Proc. IEEE Int. Conf. Commun., Control, Comput. Technol. Smart Grids*, Singapore, Oct. 2022, pp. 116–121, doi: 10.1109/SmartGridComm52983.2022.9961047.

[15] W. Huang, X. Pan, M. Chen, and S. H. Low, "DeepOPF-V: Solving AC-OPF problems efficiently," *IEEE Trans. Power Syst.*, vol. 37, no. 1, pp. 800–803, Jan. 2022, doi: 10.1109/TPWRS.2021.3114092.

[16] R. Nellikkath and S. Chatzivasileiadis, "Physics-informed neural networks for AC optimal power flow," *Electric Power Syst. Res.*, vol. 212, Nov. 2022, Art. no. 108412, doi: 10.1016/j.epsr.2022.108412.

[17] W. Liang, Y. Wang, Z. Zhao, B. Liu, and X. Li, "A data-driven AC optimal power flow using extreme learning machine," *J. Physics: Conf. Ser.*, vol. 2418, no. 1, Feb. 2023, Art. no. 012105, doi: 10.1088/1742-6596/2418/1/012105.

[18] Y. Sun, X. Fan, Q. Huang, X. Li, R. Huang, T. Yin, and G. Lin, "Local feature sufficiency exploration for predicting security-constrained generation dispatch in multi-area power systems," in *Proc. 17th IEEE Int. Conf. Mach. Learn. Appl. (ICMLA)*, Orlando, FL, USA, Dec. 2018, pp. 1283–1289, doi: 10.1109/ICMLA.2018.00208.

[19] J. S. Giraldo, M. Salazar, P. P. Vergara, G. Tsaousoglou, J. G. Slootweg, and N. G. Paterakis, "Optimal operation of community energy storage using stochastic gradient boosting trees," in *Proc. IEEE Madrid PowerTech*, Madrid, Spain, Jun. 2021, pp. 1–6, doi: 10.1109/PowerTech46648.2021.9495010.

[20] F. Diehl, "Warm-starting AC optimal power flow with graph neural networks," in *Proc. Conf. 33rd Conf. Neural Inform. Process. Syst.*, 2019, pp. 1–6.

[21] D. Owerko, F. Gama, and A. Ribeiro, "Optimal power flow using graph neural networks," in *Proc. IEEE Int. Conf. Acoust., Speech Signal Process. (ICASSP)*, Barcelona, Spain, May 2020, pp. 5930–5934, doi: 10.1109/ICASSP40776.2020.9053140.
[22] K. Baker, "Learning warm-start points for AC optimal power flow," in *Proc. IEEE 29th Int. Workshop Mach. Learn. for Signal Process. (MLSP)*, Pittsburgh, PA, USA, Oct. 2019, pp. 1–6, doi: 10.1109/MLSP.2019.8918690.
[23] S. Liu, C. Wu, and H. Zhu, "Topology-aware graph neural networks for learning feasible and adaptive AC-OPF solutions," *IEEE Trans. Power Syst.*, vol. 38, no. 6, pp. 5660–5670, Nov. 2023, doi: 10.1109/TPWRS.2022.3230555.
[24] M. Yang, G. Qiu, J. Liu, Y. Liu, T. Liu, Z. Tang, L. Ding, Y. Shui, and K. Liu, "Topology-transferable physics-guided graph neural network for real-time optimal power flow," *IEEE Trans. Ind. Informat.*, early access, May 20, 2024, doi: 10.1109/tii.2024.3398058.
[25] Q. Tran, J. Mitra, and N. Nguyen, "Learning model combining convolutional deep neural network with a self-attention mechanism for AC optimal power flow," *Electric Power Syst. Res.*, vol. 231, Jun. 2024, Art. no. 110327, doi: 10.1016/j.epsr.2024.110327.
[26] T. Falconer and L. Mones, "Leveraging power grid topology in machine learning assisted optimal power flow," *IEEE Trans. Power Syst.*, vol. 38, no. 3, pp. 2234–2246, May 2023, doi: 10.1109/TPWRS.2022.3187218.
[27] P. Wu, C. Chen, D. Lai, J. Zhong, and Z. Bie, "Real-time optimal power flow method via safe deep reinforcement learning based on primal-dual and prior knowledge guidance," *IEEE Trans. Power Syst.*, early access, Apr. 30, 2024, doi: 10.1109/TPWRS.2024.3395248.
[28] B. Feng, J. Zhao, G. Huang, Y. Hu, H. Xu, C. Guo, and Z. Chen, "Safe deep reinforcement learning for real-time AC optimal power flow: A near-optimal solution," *CSEE J. Power Energy Syst.*, early access, May 3, 2024, doi: 10.17775/CSEEJPES.2023.02070.
[29] A. Venzke, G. Qu, S. Low, and S. Chatzivasileiadis, "Learning optimal power flow: Worst-case guarantees for neural networks," in *Proc. IEEE Int. Conf. Commun., Control, Comput. Technol. Smart Grids*, Tempe, AZ, USA, Nov. 2020, pp. 1–7, doi: 10.1109/SmartGridComm47815.2020.9302963.
[30] N. Guha, Z. Wang, M. Wytock, and A. Majumdar, "Machine learning for AC optimal power flow," 2019, *arXiv:1910.08842*.
[31] R. Canyasse, G. Dalal, and S. Mannor, "Supervised learning for optimal power flow as a real-time proxy," in *Proc. IEEE Power Energy Soc. Innov. Smart Grid Technol. Conf. (ISGT)*, Washington, DC, USA, Apr. 2017, pp. 1–5, doi: 10.1109/ISGT.2017.8086083.
[32] G. Ruan, H. Zhong, G. Zhang, Y. He, X. Wang, and T. Pu, "Review of learning-assisted power system optimization," *CSEE J. Power Energy Syst.*, vol. 7, no. 2, pp. 221–231, Mar. 2021, doi: 10.17775/CSEEJPES.2020.03070.
[33] R. D. Zimmerman and C. E. Murillo-Sanchez. (2020). *MATPOWER (Version 7.1)*. [Online]. Available: https://matpower.org
[34] A. J. Wood, B. F. Wollenberg, and G. B. Sheblé, *Power Generation, Operation, and Control*. Hoboken, NJ, USA: Wiley, 2013.
[35] M. A. Pai. (1989). *IEEE 39-Bus System*. [Online]. Available: https://icseg.iti.illinois.edu/ieee-39-bus-system/
[36] S. Babaeinejadsarookolaee, A. Birchfield, R. D. Christie, C. Coffrin, C. DeMarco, R. Diao, M. Ferris, S. Fliscounakis, S. Greene, R. Huang, and C. Josz, "The power grid library for benchmarking AC optimal power flow algorithms," 2019, *arXiv:1908.02788*.
[37] ISO. *New England Demand Data*. Accessed: Apr. 17, 2023. [Online]. Available: https://www.iso-ne.com/isoexpress/web/reports/load-and-demand/-/tree/dmnd-rt-hourly-sys
[38] NASA. *Prediction of World Energy Resource*. Accessed: Apr. 17, 2023. [Online]. Available: https://power.larc.nasa.gov/

REHMAN ZAFAR (Member, IEEE) received the B.S. degree in electrical engineering from the COMSATS University Islamabad, Islamabad, Pakistan, in 2015, and the Ph.D. degree in electronics engineering from Kookmin University, Seoul, South Korea, in 2024.

He was a Graduate Researcher with Kookmin University, from 2017 to 2024, where he is currently a Postdoctoral Associate. His research interests include artificial intelligence for power system applications, renewable energy integration into the power grids, and power system control and operation.

IL-YOP CHUNG (Member, IEEE) received the B.S., M.S., and Ph.D. degrees in electrical engineering from Seoul National University, Seoul, South Korea, in 1999, 2001, and 2005, respectively.

He was a Postdoctoral Associate with Virginia Tech, Blacksburg, VA, USA, from 2005 to 2007. From 2007 to 2010, he was with the Center for Advanced Power Systems, Florida State University, Tallahassee, FL, USA, as an Assistant Scholar Scientist. He is currently a full-time Professor with the School of Electrical Engineering, Kookmin University, Seoul. His research interests include power system control and operation, renewable energy integration to power grids, remote microgrid with renewable energy, and shipboard power systems.